Synergistic Treatment of Multidrug-Resistant Bacterial Biofilms using Silver

Nanoclusters Incorporated into Biodegradable Nanoemulsions

Jungmi Park, Ahmed Nabawy⁺, Jeerapat Doungchawee⁺, Neel Mahida, Kiernan Foster, Teerapong Jantarat, Mingdi Jiang, Aritra Nath Chattopadhyay, Muhammad Aamir Hassan, Dheeraj K. Agrohia, Jessa Marie Makabenta, Richard W. Vachet, and Vincent M. Rotello*

Department of Chemistry, University of Massachusetts Amherst, 710 North Pleasant Street, Amherst, Massachusetts 01003, United States

*E-mail: rotello@chem.umass.edu

⁺ These authors contributed equally

Keywords: biofilms, antimicrobials, nanoemulsions, combination therapy, synergy, silver nanoclusters

Abstract

Multidrug resistance (MDR) in bacteria is a critical global health challenge that is exacerbated by the ability of bacteria to form biofilms. We report a combination therapy for biofilm infections that integrates silver nanoclusters (AgNCs) into polymeric biodegradable nanoemulsions (BNE) incorporating eugenol. These Ag-BNEs demonstrated synergistic antimicrobial activity between the AgNCs and the BNE. Microscopy studies demonstrate that Ag-BNE penetrated the dense biofilm matrix and effectively disrupted the bacterial membrane. The Ag-BNE vehicle also resulted in more effective silver delivery into the biofilm than AgNCs alone. The disruption provided by the BNE and enhanced delivery of AgNCs into the biofilm combined synergistically to provide highly efficient killing of MDR biofilms.

Introduction

Multidrug-resistant (MDR) bacterial infections affect more than 2.8 million patients in the U.S. annually, with the mortality rates of these infections predicted to surpass cancer by 2050. 1,2

1

The challenge presented by MDR bacteria is further aggravated by the ability of these bacteria to induce biofilm infections.^{1,3} The dense structure of the bacterially-excreted extracellular polymeric substances (EPS) can limit the penetration of host immune cells as well as antibiotics, allowing prolonged survival of bacteria.⁴ The National Institutes of Health (NIH) estimates that biofilm-associated infections account for more than 80% of recurrent and chronic microbial infections.² These infections are serious on their own and can cause serious complications such as sepsis when bacteria are released from the biofilm into the bloodstream.^{4,5}

Treatment of biofilm infections using conventional antibiotics and antimicrobials is challenging. Bacteria residing inside the matrix can be protected from antibiotics both physically and metabolically, resulting in the development of tolerance and resistance.^{6,7,8,9} Nature-derived essential oils are promising antimicrobial agents, showing broad-spectrum bactericidal activity.^{10,11,12} Essential oils have several advantages as antibiotic alternatives such as low cost,¹³ general safety ¹⁴, and delayed resistance development. ¹⁵ However, these oils are generally ineffective against biofilm infections due to their poor aqueous solubility and inability to penetrate the EPS matrix. ¹⁶ Amphiphilic nanomaterials can stabilize and deliver hydrophobic essential oils. ^{17,18,19,20} These platforms have also been used to deliver essential oils combined with other small-molecule antimicrobials to combat planktonic and biofilm infections. ^{21,22}

Combination therapy using two or more antimicrobial agents can provide enhanced treatment of MDR bacterial infections.²³ Appropriate choice of therapeutic agents can even provide a synergistic activity that surpasses that of the individual agents.^{24, 25} Polymers are strategically poised as platforms for combination antimicrobial therapies, building on the vast design space of polymer architectures.²⁶

Silver (Ag)-based materials are particularly effective antibacterial agents, exerting broad-spectrum antimicrobial properties through multiple mechanisms. Ag $^+$ ions released from these materials adhere to the cell wall and cytoplasmic membrane, leading to the disruption of the bacterial envelope. 27,28 Ultrasmall (≤ 2 nm) Ag nanoclusters (AgNCs), are widely employed for biomedical applications due to their high surface-to-volume ratio and ready functionalization. 29,30,31 Challenges remain, however, in delivering AgNCs into biofilms. 32

We hypothesized that essential oil-based nanoemulsions ^{33,34} could transport ultrasmall AgNCs into biofilms for efficient co-delivery with the essential oil, providing an effective combination therapy. AgNCs were loaded into biodegradable polymeric nanoemulsions (BNE) through incorporation of hydrophobically-modified AgNCs into the eugenol oil phase (Figure 1). These dual-antimicrobial Ag-BNE nanomaterials demonstrated broad-spectrum activity against four different pathogenic MDR strains: *E. coli*, *A. baumannii*, *P. aeruginosa*, and methicillin-resistant *S. aureus* (MRSA). Significantly, the activities of the essential oil and the AgNCs were synergistic, with the Ag-BNE having up to a 4-fold decrease in minimum biofilm bactericidal concentrations (MBBCs) compared to the individual therapeutic agents. Inductively coupled plasma mass spectrometry (ICP-MS) imaging showed that one origin of this synergy was enhanced delivery of Ag into the biofilm. Overall, the integration of AgNCs into nanoemulsions provides a highly effective synergistic strategy to combat life-threatening MDR biofilm infections.

Results and Discussion

Fabrication of Ag-BNEs. The polymer component of Ag-BNE nanoemulsions was engineered with an amphiphilic poly(oxanorbornenimide) (PONI)-based scaffold that generates nanoemulsions through interacting with hydrophobic cargos.¹⁹ The PONI random copolymer is

polymerized with functional monomer units with three different side chains: cationic guanidinium, maleimide, and tetraethylene glycol monoethyl ether (TEG). The positively charged guanidinium groups provide an overall positive charge on the nanoemulsions, enhancing interaction and penetration of negatively charged bacterial membranes and biofilms.^{17, 18} TEG side chains increased amphiphilicity of the polymers, enabling stabilization of oil payload. Finally, maleimide moieties were used to cross-link via maleimide-Michael addition with a dithiol-disulfide cross-linker (DTDS) at physiological pH 6.5 – 7.5 (Figure 1b). ¹⁹ Among essential oils, eugenol has shown broad-spectrum of antimicrobial activity by lipid fraction of the bacterial membrane,³⁵ as well as in the class of generally recognized as safe (GRAS) by FDA.³⁶ The BNE nanoemulsions were formed using eugenol which was also demonstrated to induce significant synergistic activities with other antimicrobials such as colistin or nanoparticles.^{37,38, 39,40}

Hydrophobic AgNCs are compatible with the eugenol oil phase of the BNE platform were prepared using a phase transfer method. Transfer of AgNCs to the organic phase was achieved using the cationic aliphatic ligand dodecyl trimethylammonium bromide (DTAB). 30,41,42 DTAB was added and vigorously mixed between organic layer with DTAB and AgNCs in aqueous layer (Figure 1a). The UV-Vis absorption spectrum of oil-soluble AgNCs obtained from the organic layer was characterized in chloroform by three absorption peaks (330, 420, and 500 nm) (Figure S1) consistent with previously reported phase-transferred AgNCs. The hydrophobic AgNCs were vacuum dried to ensure the removal of chloroform. The AgNCs dissolved in eugenol efficiently (up to 66 mg/mL) allowing efficient loading of AgNCs into the BNE platform.

The AgNC-loaded eugenol was emulsified with aqueous PONI-GMT solutions using a commercially available amalgamator to afford AgNC-loaded nanoemulsions (Ag-BNE). Dynamic light scattering (DLS) measurement confirms the formation of nanoemulsions with a diameter of

~150 nm with narrow size distribution (PDI: 0.104) (Figure 1c). The nanoemulsions were visualized under transmission electron microscopy (TEM) and presented a spherical morphology with a similar size (120 nm) as observed from DLS (Figure 1d, Figure S2).

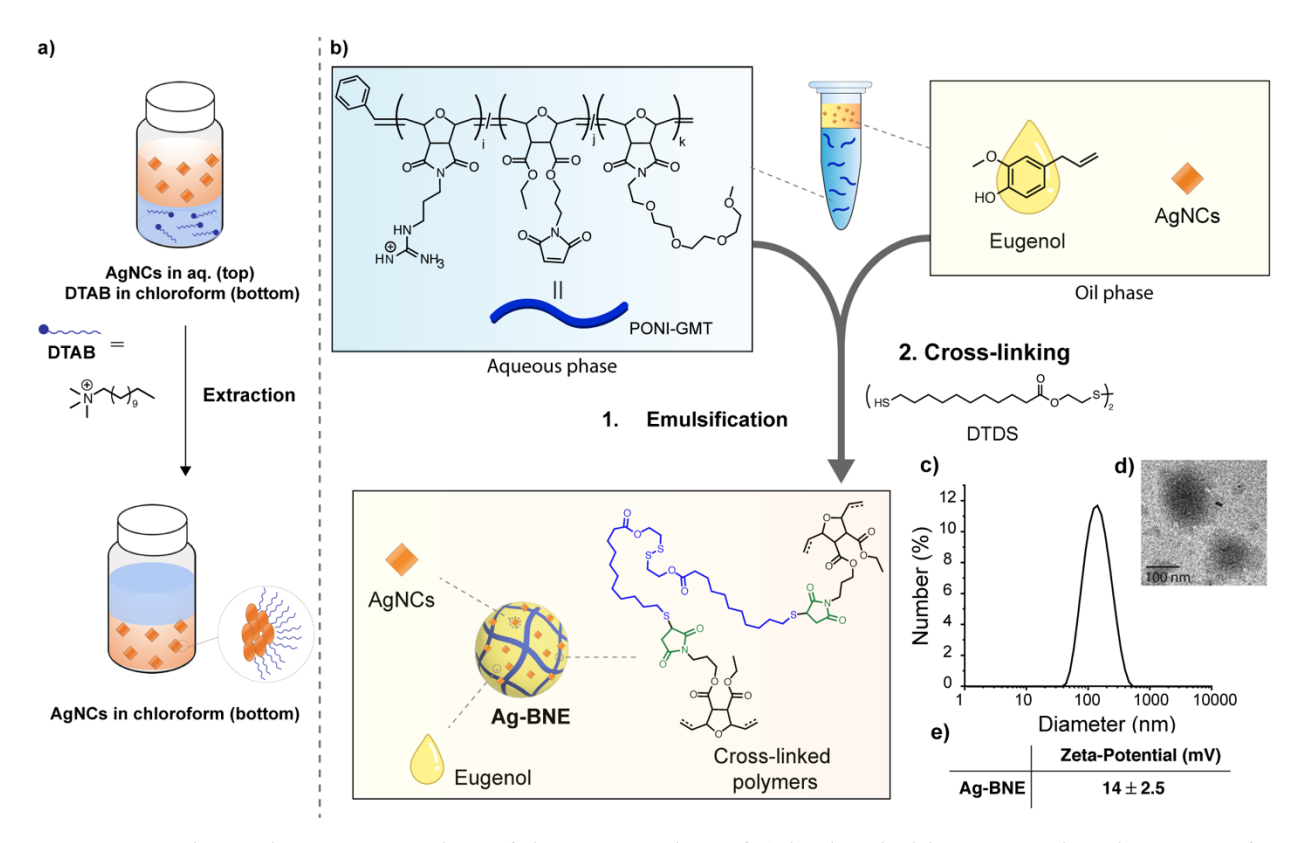


Figure 1. Schematic representation of the preparation of a) hydrophobic AgNCs by phase transfer method and b) Ag-BNE (i:j:k = 4:5:1). Characterization of Ag-BNE including c) dynamic light scattering (DLS) histogram of Ag-BNE in PBS buffer d) Transmission electron microscopy image and e) Zeta-potential of Ag-BNE.

Ag-BNEs show potent killing of pathogens in biofilms. The antibacterial activity of Ag-BNEs was first evaluated *in vitro* against two pathogens producing clinically challenging biofilms; MRSA (IDRL-6169) and *P. aeruginosa* (CD-1006). Biofilms were grown for 2 days, and with scanning electron microscopy (SEM) indicating formation of bacterial biofilms (Figure S3). The bacterial viability was measured via Alamar blue assay after 3 h treatment with each group AgNCs, BNE and Ag-BNE. Ag-BNEs featured high antimicrobial activity against mature 2-day-old

biofilms (Figure 2). The Ag-BNEs were substantially more effective than BNEs and AgNCs separately even at low concentrations of AgNCs as of 1 mg/L (Figure 2). Notably, Ag-BNEs were effective against both Gram-negative and Gram-positive bacterial biofilms. In contrast, BNEs had modest activity against MRSA biofilms and dose-dependent antibiofilm effect against *P. aeruginosa* biofilms. AgNCs showed antibiofilm activity in MRSA biofilms, but little antibiofilm activity in *P. aeruginosa*, possibly due to different acts of mechanisms of two antimicrobial systems.

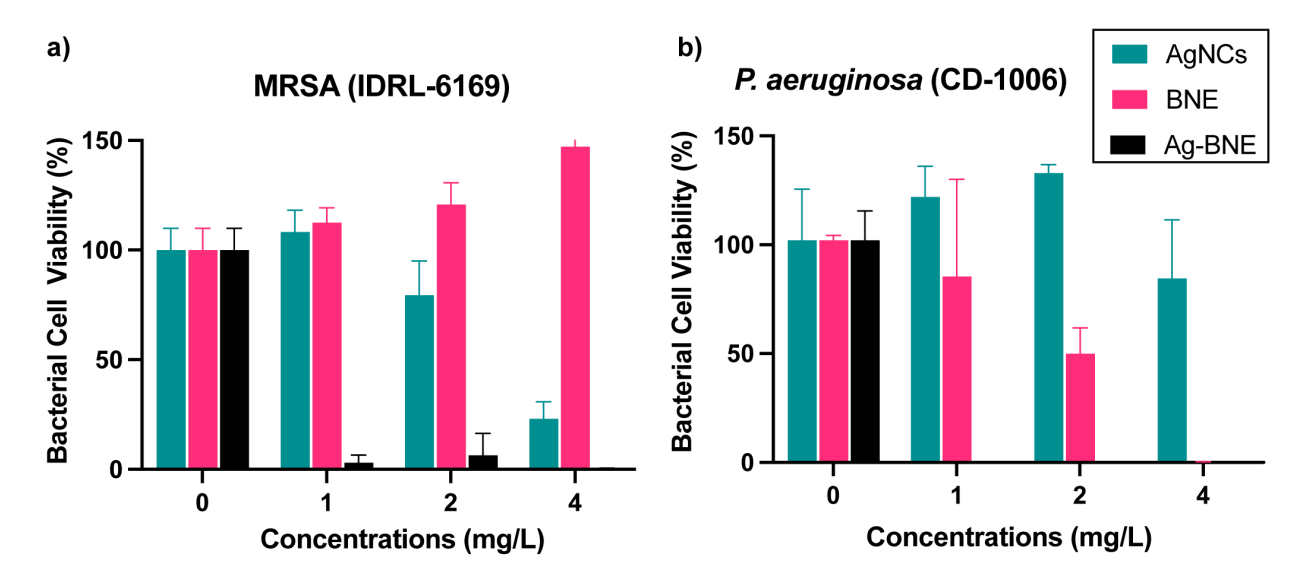


Figure 2. Antimicrobial efficacy of Ag-BNEs, BNEs, and AgNCs against pathogenic bacterial biofilms established as described in the experimental section. Cell viability results as of concentrations of AgNCs (mg/L) a) *P. aeruginosa* and b) MRSA by Alarma blue assay. Values are expressed as mean \pm standard deviation of \geq 3 replicates in two repeated experiments.

Ag-BNE provides synergistic killing of biofilm bacteria. Combination therapies can present three different interactions between components: synergy, additivity, or antagonism.⁴³ Synergy increases treatment efficacy by decreasing the required dosing of therapeutics. Interactions between therapeutics can be quantified using by the fractional inhibitory (FIC) index, with FIC values <0.5 considered synergy. ⁴⁴ The antimicrobial synergy between AgNCs and eugenol in the

Ag-BNE was tested against four clinically isolated bacteria strains: *A. baumannii* (CD-575), MRSA (IDRL-6169), *E. coli* (CD-2), and *P. aeruginosa* (CD-1006).

First, the minimum biofilm bactericidal concentration (MBBC) was determined for each component. The eugenol BNEs were used as prepared. AgNCs were dissolved in DMSO, with DMSO levels in solution < 10%. Checkboard titrations^{45,46} were performed with varying AgNCs within Ag-BNE (Figure 3a-d) by microdilution methods. The FIC index was calculated to evaluate specific effects of these combinations against each bacterial strain (Figure 3e). Synergy (FIC indices \leq 0.5) between AgNCs and eugenol was observed for two strains, *A. baumannii* (CD-575) and MRSA (IDRL-6169). Indifferent (weak synergy or additivity, FIC indices of \leq 1) behavior was observed with *E. coli* (CD-2) *and P. aeruginosa* (CD-1006). Overall, there was a 4- to 16-fold reduction in MBBCs of Ag-BNE compared to a single treatment. The synergistic activity of the Ag-BNE platform demonstrates the promise of combination therapy through nanoemulsion-assisted delivery of AgNCs.

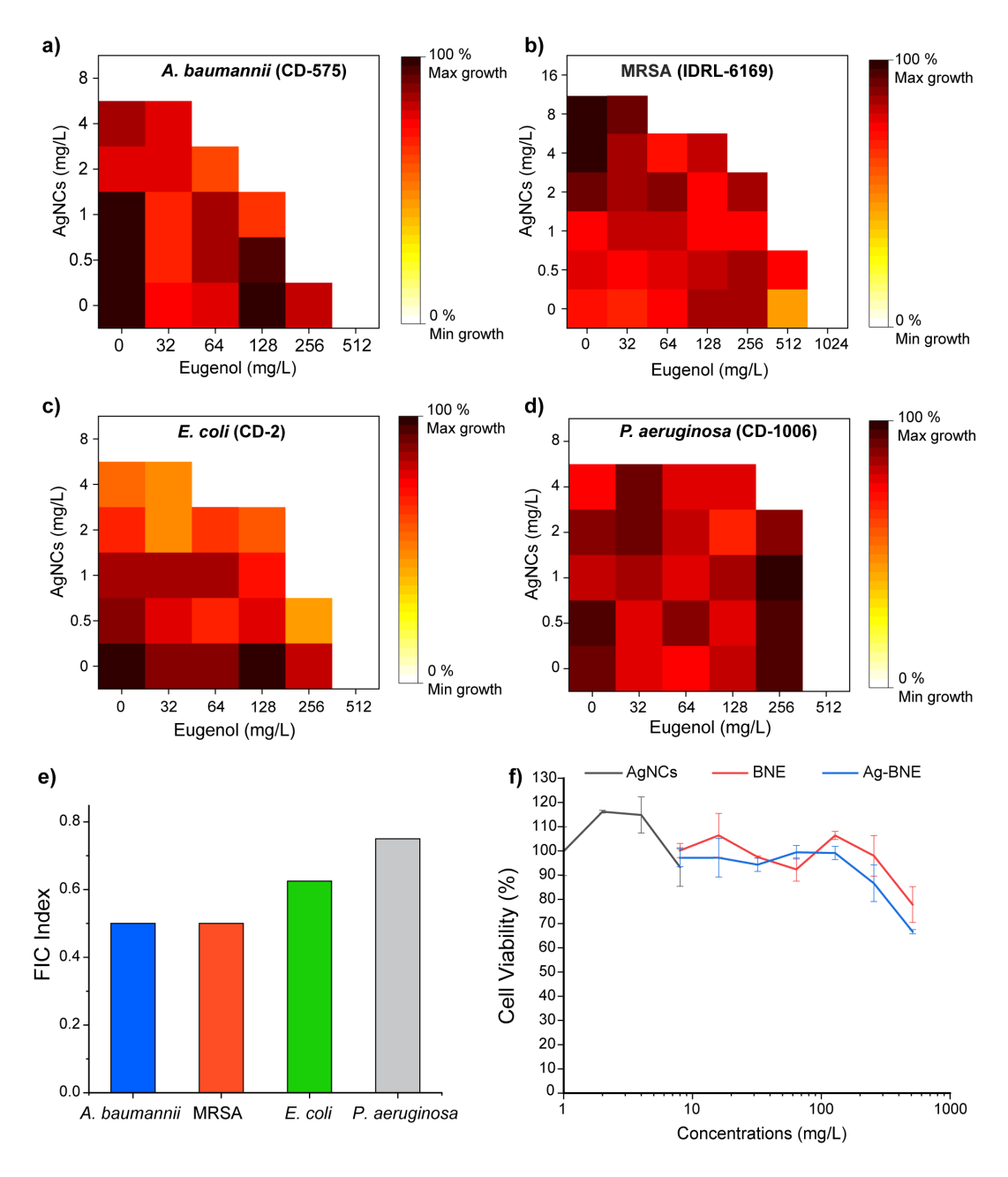


Figure 3. a-d) Checkerboard microdilution assay for minimal biofilm bactericidal concentration (MBBC) against *A. baumannii* (CD-575), methicillin-resistant *S. aureus* (IDRL-6169), *E. coli* (CD-2), *P. aeruginosa* (CD-1006) e) Fractional inhibitory concentration (FIC) indices to assess synergy between BNE and AgNCs in eradicating biofilm. FIC values ≤0.5 correspond to synergistic combinations. f) Viability of human fibroblast cells (ATCC CRL-1658) after 3 h exposure to AgNCs, BNE, and Ag-BNE. Values are expressed as mean \pm standard deviation of ≥3 replicates.

Ag-BNEs are non-toxic to mammalian cells. Next, we determined the effects of AgNCs, BNEs, and Ag-BNEs on a human fibroblast cell line (ATCC CRL-1658), a cell type relevant to wound healing. 47 Viability was determined using the Alamar blue assay. As shown in Figure. 3f, AgNCs, BNE, and Ag-BNE showed little effect on cellular viability at concentrations effective against MDR biofilms. Hemolysis assays were performed with human red blood cells. Similar to Alamar blue results, Ag-BNE did show hemolytic activity (Fig. S4), emphasizing the potential of this combination therapy strategy.

Ag-BNEs penetrate biofilms and kill bacteria through membrane disruption. Confocal microscopy was used to probe antimicrobial mechanisms accessed by Ag-BNEs. Live/dead membrane integrity staining was used to visualize activity. SYTO 9 (Thermo Fisher) enters both live and dead cells while propidium iodide (PI) only enters bacteria with compromised cell membranes. In practice, two-day-old MRSA biofilms were treated with Ag-BNE for 2 hours and then stained with SYTO 9 (green) and PI (red). Untreated cells showed no staining by PI. In contrast, bacteria throughout the biofilm treated with Ag-BNEs were stained red by PI (Figure 4). Co-localization of this red fluorescence with the green signal from the SYTO 9 confirms biofilm penetration and bacterial membrane disruption by Ag-BNEs throughout the biofilm.

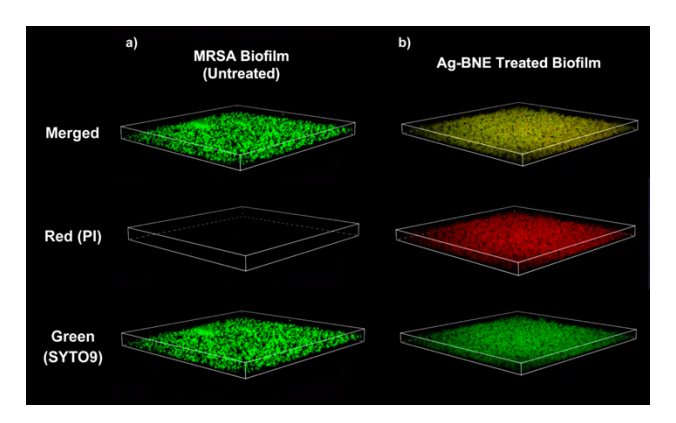


Figure 4. CLSM images of MRSA biofilm stained by PI and SYTO 9 a) untreated and b) treated with Ag-BNE for 2 h as representative 3D views of images of 2-day MRSA biofilms after 3 h incubation. The dead cells were visualized by PI staining (red) and SYTO 9 (green) stained both live/dead cells.

Synergy through BNE-enhanced delivery of Ag into biofilms. We hypothesized that the synergistic activity of AgNCs resulted from BNE-enhanced penetration of the AgNCs into biofilms. The efficiency of Ag penetration into biofilm was quantified using inductively coupled plasma mass spectrometry (ICP-MS). For these studies, four-day biofilms of 1) *P. aeruginosa* (CD-1006) and 2) MRSA (IDRL-6169) were established and treated with AgNCs and Ag-BNE. Based on the observed MBBC of 4 mg/L of AgNCs in Ag-BNE, *S. aureus* and *P. aeruginosa* biofilms were treated with 1-8 mg/L of Ag-BNE (by AgNC) and AgNCs. After 1 h, treated and untreated biofilms were collected and digested using HNO₃:H₂O₂. The ICP-MS analysis revealed that higher uptake of Ag was observed in the Ag-BNE sample compared to AgNCs alone (Figure 5a-c). The normalized uptake revealed *S. aureus* biofilm uptake of Ag ~1.5 times higher in *S. aureus* than *P. aeruginosa*, providing a rationale for the enhanced synergy seen with MRSA.

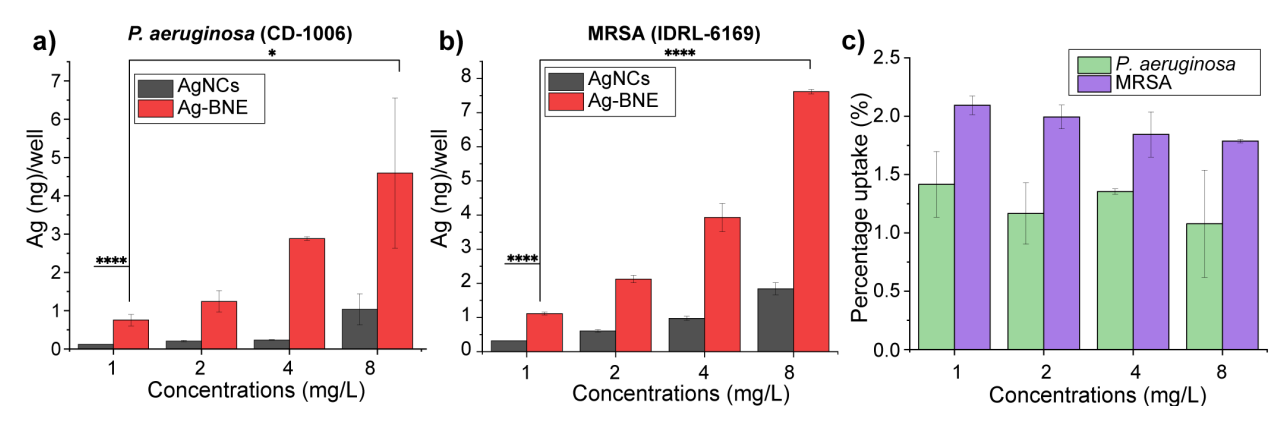


Figure 5. Quantification of silver (Ag) ions by ICP-MS after treatment with varying concentrations of AgNCs and Ag-BNE of a) P. aeruginosa and b) MRSA biofilm. c) Comparison of percentage uptake of Ag in P. aeruginosa and MRSA biofilm. Values are expressed as mean \pm standard deviation of \geq 3 replicates. A difference was considered significant if the p-value, * p <0.05, **** p<0.0001 calculated by performing an unpaired t-test.

LA-ICP-MS imaging shows co-localization of Ag and Zn deprivation after treatment with

Ag-BNE. Zinc ions (Zn) are associated with biofilm-associated proteins and provide a mass spectrometric marker for biofilm health. ^{50,51} The Zn and Ag distribution of individual biofilms were quantified by LA-ICP-MS imaging. The treated and untreated biofilms were washed three times with PBS to remove any free-floating materials and dried before the imaging experiment. LA-ICP-MS images showed a marked decrease of Zn signal in Ag-BNE treated biofilm compared to non-treated biofilm, indicating the disruption of biofilm (Figure 6a-d). LA-ICP-MS images also showed the distribution of Ag from the system and co-localized with Zn signal in biofilm, corresponding to a strong correlation of Ag and Zn. (Pearson's correlation coefficient >0.5, p-value <0.05, Figure S4). Ag intensity is significantly increased in 8 mg/L Ag-BNE treated sample relative to 4 mg/L (p-value <0.01), with more co-localized distribution in 8 mg/L Ag-BNE treated biofilms (Figure 6e). These studies are consistent with disruption of biofilms and/or inhibition of their growth by Ag⁺.

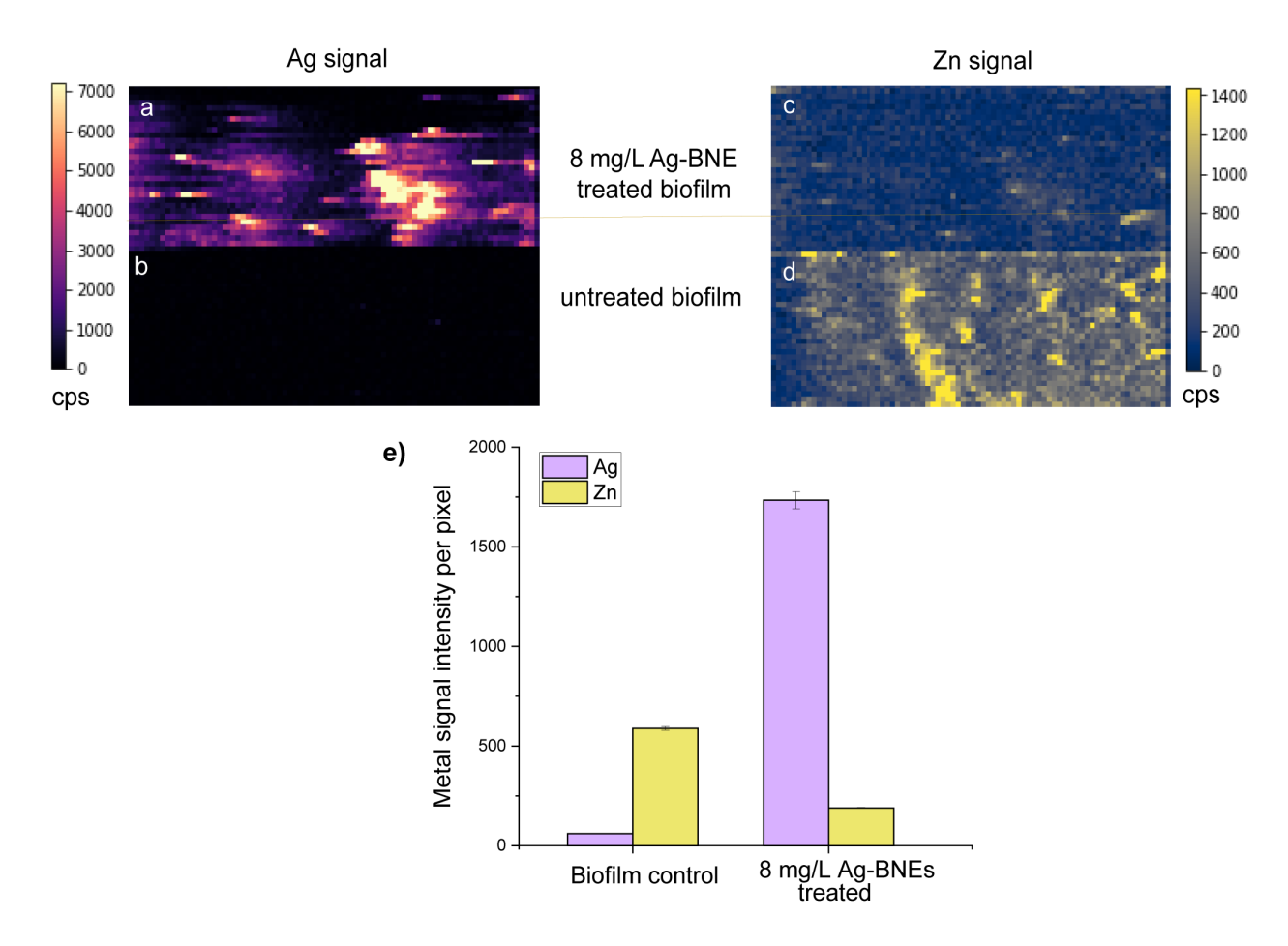


Figure 6. Representative LA-ICP-MS images at 50 μm resolution of methicillin-resistant *S. aureus* (MRSA) biofilm after 1h of incubation a) and c) treated with 8 mg/L Ag-BNE b) and d) no treatment. e) Ag and Zn signal intensity per pixel in individual biofilm samples.

Conclusions

In summary, we created dual-mode therapeutic Ag-BNE nanoemulsions that combine the antimicrobial activity of essential oils with that of silver ions. The antimicrobial hybrid displayed synergistic activity, with a 4 to 16-fold decrease in MBBC compared to treatment with the components separately. The efficacy of Ag-BNE was attributed to enhanced biofilm penetration as demonstrated by bacterial membrane disruption within biofilms. ICP-MS studies support the hypothesis that synergy arose from enhanced penetration of the AgNCs into the biofilm from the

nanoemulsion. Taken together, this system provided a potent combination therapeutic platform for integrating essential oils and silver-based nanomaterials to treat bacterial biofilm infections.

Experimental Section

Synthesis of oil-soluble AgNCs by phase transfer. Water-soluble AgNCs were prepared by a modification of a previously reported method.²⁹ To a purified water-soluble AgNCs 10 mL of an aqueous solution of 4 mg of AgNCs in MQ water was mixed with 5 mL of a chloroform solution of dodecyl trimethylammonium bromide (DTAB) (containing 1.2 mg of the solute). The two layers were vigorously shaken and AgNCs were extracted into the organic phase by observing the orange color in the organic layer. The organic layer was separated and dried, and 3 mL of ethanol was added to it for further washing to rinse out excess ligands. The mixture obtained was stirred vigorously for 1 min using a vortex mixer and centrifuged at 6000 rpm for 10 min. The mixture was vacuum-dried to obtain solid AgNCs and stored at a cool temperature until further use.

Preparation of Ag-BNE. Ag-BNE was prepared through emulsification of eugenol (loaded with AgNCs and DTDS) into an aqueous PONI-GMT solution. The solid AgNCs were dissolved in eugenol at varying concentrations up to 66 mg/mL with DTDS (3 wt %). Next, 3 μ L of the oil mixture and 497 μ L of PONI-GMT in aqueous solution were added. This resulting mixture was then emulsified for 50 s using an amalgamator. Emulsions were allowed to rest overnight before use.

Biofilm formation and treatment. Bacteria from stock agar plates were inoculated in TSB broth at 37 $^{\circ}$ C until they reached the log phase. Grown bacteria were harvested by centrifugation and washed with 0.85% sodium chloride solution three times. Concentrations of resuspended bacteria were determined by optical density measured at 600 nm. Seeding solutions were made in TSB to an OD 600 of 0.1. 100 μ L of the seeding solutions were added to each well of a microtiter well

plate. TSB medium without bacteria was used as a negative control. Plates were covered and incubated at room temperature under static conditions for desired periods (2 days or 4 days). Planktonic bacteria were removed by washing with phosphate-buffered saline (PBS) three times. The washed biofilm was treated with materials for 3 hours at 37 °C. Treated biofilms were washed with PBS and bacterial cell viability was determined using an alamarBlue Cell Viability Reagent assay (Invitrogen, US) in triplicate. The experiment was repeated twice separately, and the results were recorded.

Propidium Iodide/SYTO 9 Staining Assay. To the treated and rinsed biofilms as mentioned above, propidium iodide (PI) and SYTO 9 in M9 were added with 1.65 μM and 10 μM respectively. The samples were observed with a confocal laser scanning microscopy, Nikon A1 resonant scanning confocal with a TIRF module. Images were processed using NIS-Elements software.

Minimal Biofilm Bactericidal Concentration (MBBC) determination. The MBBCs for the AgNCs, BNEs, and Ag-BNE were determined using previously established protocols. Briefly, bacterial cells from overnight cultures were diluted to 1/50 th using tryptic soy broth (TSB) and incubated at 275 rpm, 37 °C until they reached the mid-log phase. Then, 150 μL of bacteria culture was added to each well of a 96-well microtiter plate with pegged lids and incubated for 6 h at 37 °C at 50 rpm. Then, the pegged lid was submerged in 200 μL PBS for 30 seconds for rinsing and transferred to a plate containing two-fold serial dilutions of therapeutics prepared in a separate 96-well plate using M9 media (5% TSB in M9 for G-(+)). The plate was incubated at 37 °C for 24 h. Then, treated biofilms on the lid as described above with PBS and transferred to a new plate containing fresh media. The plate was further incubated at 37 °C to determine the MBBC. The MBBC of both antibiofilm agents was determined by visual inspection and confirmed through

spectrophotometry (OD_{600}). The experiment was repeated three times separately, and the results were recorded.

Checkerboard titration for synergy testing. 2D checkerboard titrations were performed using broth micro-dilution to assess for synergy between AgNCs and BNE against biofilms. Concentrations of BNE and Ag-BNE were varied using two-fold serial dilutions according to their MIC against the respective bacterial biofilms. After treatment, wells were observed visually and recorded for any visual growth. The clear wells as compared to growth controls were considered as combinations that eliminate biofilm formation. OD₆₀₀ values were measured for confirmation of the clearance of wells. Synergy was evaluated by calculating the FIC index according to this formula:

$$FIC_{Ag} = (MBBC \text{ of } Ag-BNE \text{ combination}) \div (MBBC \text{ of } AgNCs \text{ alone})$$

$$FIC_{BNE} = (MBBC \text{ of Ag-BNE combination}) \div (MBBC \text{ of BNE alone})$$

$$FIC index = FIC_{Ag} + FIC_{BNE}$$

FIC index values ≤0.5 correspond to synergy, FIC index between 0.5 and 1 correspond to additive, FIC index values between 1 and 4 correspond to difference, and FIC index >4 correspond to antagonism.

Mammalian cell viability assay. Cytotoxicity of different components was assessed using previously established protocols.¹⁷ Briefly, 20000 NIH 3T3 fibroblast cells (ATCC CRL-1658) were cultured in Dulbecco's modified Eagle medium (DMEM, ATCC 30–2002) with 1% antibiotics and 10% bovine calf serum in a humidified atmosphere of 5% CO₂ at 37 °C for 48 h in a 96-well plate. After 24 h, media was removed and cells were washed with phosphate-buffered saline (PBS) before incubation with therapeutics. agents, BNE or Ag-BNE solution was prepared in 10% serum-containing media and incubated with cells in a 96-well plate for 3h in a humidified

atmosphere at 37 °C. Alamar blue assays were performed to assess cell viability following the manufacturer's protocol of Invitrogen Bio-source. Red fluorescence from the reduction of the Alamar blue agent was quantified using a Spectromax M5 microplate reader (Ex: 560 nm, Em: 590 nm) and used to determine cell viability in percentage. Cells incubated with no materials were considered 100% viable controls. Each experiment was performed in triplicate and repeated on two different days.

Hemolysis Assay. The hemolysis assay was conducted using human whole blood purchased from BioIVT Elevating Science. Red blood cells were separated through centrifugation at 5000 rpm for 5 minutes and washed four times with PBS buffer. The red blood cells were then diluted in PBS to achieve a final concentration of approximately 5% (v/v). Ag-BNEs were diluted in PBS using serial dilution and added to 96-well plates (200 μL per well). Subsequently, a suspension of the diluted blood cells (20 μL per well) was added to each well. The plates were then incubated at 37°C for 1 hour while being shaken at 150 rpm. Negative control samples contained PBS, while positive control samples contained Triton X-100 (0.1%). Following the incubation period, the mixture in each well was centrifuged at 3000 rpm for 7 minutes. Next, 120 μL of the resulting supernatant was transferred to a new 96-well plate. The absorbance of each well was measured at 560 nm, and the degree of hemolysis was determined using the provided formula.

Hemolysis =
$$\frac{\text{OD } 560_{\text{Sample}} - \text{OD } 560_{\text{PBS}}}{\text{OD } 560_{\text{Triton}} - \text{OD } 560_{\text{PBS}}} \text{ X } 100$$

Biofilm digestion for ICP-MS.

A silver calibration curve was made using a silver standard solution (PerkinElmer Pure 1000 mg/L Silver in 2% HNO₃). The calibration standards also contain iridium as an internal standard. These calibration standards were used in the subsequent experiments AgNCs samples at different approximated concentrations. Aliquots of these samples were taken and diluted to make 2 %

solutions, iridium, and *aqua regia** (1:3 v/v nitric acid to hydrochloric acid) were added and were then analyzed in ICP-MS to determine an accurate concentration of Ag. 4-day-old *P. aeruginosa* and MRSA biofilms grown in 96-well plates and treated with various concentrations of AgNCs solutions, as well as those treated with Ag-BNE, and controls, biofilms treated with BNE only or biofilm only as negative controls. These samples were rinsed with PBS to remove any excess materials and digested using a 1:3 mixture of H₂O₂ and H₂SO₄. Then, the samples were transferred into individual 15 mL conical tubes. The wells were rinsed with aqua regia and Millipore water. To prepare the samples for ICP-MS analysis, an internal standard was added, then the samples were diluted to 2 mL. The samples were analyzed using ICP-MS and quantified using the Ag standard calibration curve, as well as another calibration curve made using blank biofilm samples spiked. This experiment was then repeated with a gram-positive biofilm, MRSA. Using mass spectrometric imaging, gelatin calibration standards were prepared and sliced to make a calibration curve. Any statistical analysis done on the data was done in R Studio.

*Warning: Aqua regia is an extremely corrosive and strong oxidizing agent; it must be handled in proper personal protective equipment in order to be handled safely.

Acknowledgments

This research was supported by the National Institutes of Health under R01 AI134770 and NSF CHE-2108044. The content is solely the responsibility of the authors and does not necessarily represent the official views of the National Institutes of Health. Clinical isolates, *P. aeruginosa* (CD-1006), *A. baumannii* (CD-575), and *E. coli* (CD-2) obtained from the Infectious Diseases Research Laboratory at Mayo Clinic, were kindly provided by Dr. Robin Patel. Clinical samples were obtained from the Cooley Dickinson Hospital Microbiology Laboratory (Northampton, MA) and were kindly provided by Dr. Margaret Riley. Clinical isolate, methicillin-resistant *S. aureus*

(IDRL-6169), was from the Infectious Diseases Research Laboratory at Mayo Clinic, kindly provided by Dr. Robin Patel. The microscopy data was gathered in the Light Microscopy Facility and Nikon Center of Excellence at the Institute for Applied Life Sciences.

Author Contributions

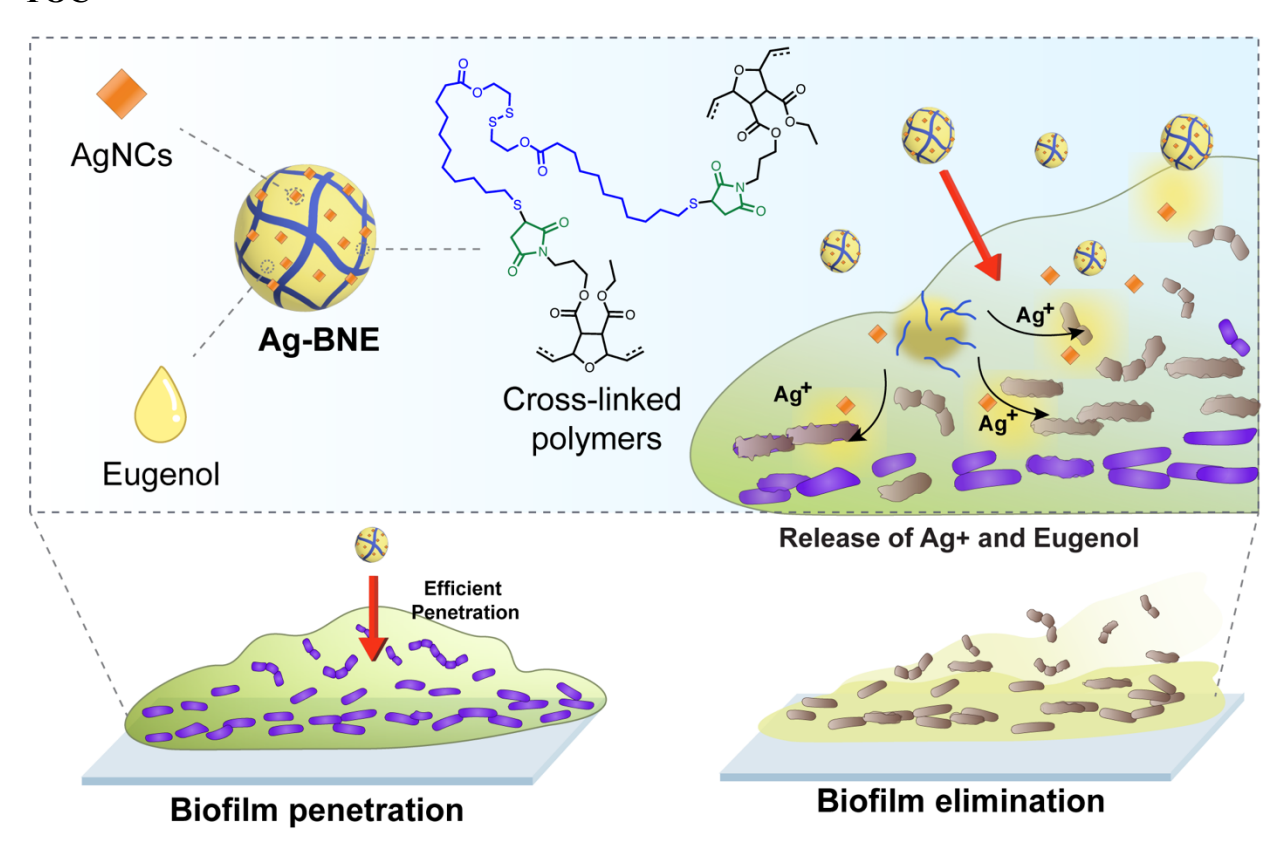
The manuscript was written through contributions of all authors. J.P., A.N. and R.W.V., V.M.R. conceived the idea and designed the experiments. J.P. synthesized and characterized materials. J.P. and J.D. designed the mass spectrometry experiments, and J.D., K.F., T.J., and D.K.A. performed ICP-MS and related analyses. J.P., N.M., and M.A.H. performed in vitro biofilm studies and related analyses. J.M.M. provided help in confocal imaging and analysis. M.J. cultured mammalian cells and performed in vitro cell studies and related analyses. A.C. performed TEM imaging. All authors discussed results and provided suggestions for the manuscript. All authors have approved the final version of the manuscript. ‡These authors contributed equally.

Supporting Information

Supporting information includes materials and methods, optical spectra of AgNCs, TEM image of Ag-BNE, SEM image of biofilm, hemolysis assay for Ag-BNE and LA-ICP-MS Image overlays of Ag and Zn in individual biofilms.

1

TOC



Schematic representation of AgNCs-loaded biodegradable polymeric nanoemulsions (Ag-BNE) effectively penetrating the biofilm, releasing dual antimicrobials Ag⁺ and eugenol and lysing bacteria cells.

References

1. Shankar, Pr. Book Review: Tackling Drug-Resistant Infections Globally. *Arch. Pharm. Pract.* **2016**, 7 (3), 110.

- 2. Dadgostar, P. Antimicrobial Resistance: Implications and Costs. *Infect. Drug Resist.* **2019**, *12*, 3903–3910.
- 3. Vestby, L. K.; Grønseth, T.; Simm, R.; Nesse, L. L. Bacterial Biofilm and Its Role in the Pathogenesis of Disease. *Antibiotics* **2020**, *9* (2).
- 4. Bjarnsholt, T. The Role of Bacterial Biofilms in Chronic Infections. *APMIS. Suppl.* **2013**, No. 136, 1–51.
- 5. Jamal, M.; Ahmad, W.; Andleeb, S.; Jalil, F.; Imran, M.; Nawaz, M. A.; Hussain, T.; Ali, M.; Rafiq, M.; Kamil, M. A. Bacterial Biofilm and Associated Infections. *J. Chinese Med. Assoc.* **2018**, *81* (1), 7–11.
- 6. Stewart, P. S.; Franklin, M. J. Physiological Heterogeneity in Biofilms. *Nat. Rev. Microbiol.* **2008**, *6* (3), 199–210.
- 7. Kalhapure, R. S.; Suleman, N.; Mocktar, C.; Seedat, N.; Govender, T. Nanoengineered Drug Delivery Systems for Enhancing Antibiotic Therapy. *J. Pharm. Sci.* **2015**, *104* (3), 872–905.
- 8. Singh, R.; Sahore, S.; Kaur, P.; Rani, A.; Ray, P. Penetration Barrier Contributes to Bacterial Biofilm-Associated Resistance against Only Select Antibiotics, and Exhibits Genus-, Strain- and Antibiotic-Specific Differences. *Pathog. Dis.* **2016**, *74* (6), 1–6.
- 9. Tran, H. M.; Tran, H.; Booth, M. A.; Fox, K. E.; Nguyen, T. H.; Tran, N.; Tran, P. A. Nanomaterials for Treating Bacterial Biofilms on Implantable Medical Devices. *Nanomaterials* **2020**, *10* (11), 1–19.
- 10. D'agostino, M.; Tesse, N.; Frippiat, J. P.; Machouart, M.; Debourgogne, A. Essential Oils and Their Natural Active Compounds Presenting Antifungal Properties. *Molecules* **2019**, *24* (20).
- 11. Gutierrez, J.; Barry-Ryan, C.; Bourke, P. The Antimicrobial Efficacy of Plant Essential Oil Combinations and Interactions with Food Ingredients. *Int. J. Food Microbiol.* **2008**, *124* (1), 91–97.
- 12. Dhifi, W.; Bellili, S.; Jazi, S.; Bahloul, N.; Mnif, W. Essential Oils' Chemical Characterization and Investigation of Some Biological Activities: A Critical Review. *Medicines* **2016**, *3* (4), 25.
- 13. Susilo, B.; Lestari W. H, M.; Rohim, A. Impact of Using Low-Cost Packaging Material of Commercial Herbal Oil on Its Antibacterial Compounds. *All Life* **2020**, *13* (1), 516–523.
- 14. Johnson S; Boren K. Topical and Oral Administration of Essential Oils-Safety Issues. *Aromatopia* **2013**, *22* (4), 43–48.
- 15. Santos, M. I. S.; Marques, C.; Mota, J.; Pedroso, L.; Lima, A. Applications of Essential Oils as Antibacterial Agents in Minimally Processed Fruits and Vegetables—A Review. *Microorganisms* **2022**, *10* (4), 1–24.
- 16. El-Tarabily, K. A.; El-Saadony, M. T.; Alagawany, M.; Arif, M.; Batiha, G. E.; Khafaga, A. F.; Elwan, H. A. M.; Elnesr, S. S.; E. Abd El-Hack, M. Using Essential Oils to Overcome Bacterial Biofilm Formation and Their Antimicrobial Resistance. *Saudi J. Biol. Sci.* **2021**, *28* (9), 5145–5156.

- 17. Li, C. H.; Chen, X.; Landis, R. F.; Geng, Y.; Makabenta, J. M.; Lemnios, W.; Gupta, A.; Rotello, V. M. Phytochemical-Based Nanocomposites for the Treatment of Bacterial Biofilms. *ACS Infect. Dis.* **2019**, *5* (9), 1590–1596.
- 18. Landis, R. F.; Li, C. H.; Gupta, A.; Lee, Y. W.; Yazdani, M.; Ngernyuang, N.; Altinbasak, I.; Mansoor, S.; Khichi, M. A. S.; Sanyal, A.; Rotello, V. M. Biodegradable Nanocomposite Antimicrobials for the Eradication of Multidrug-Resistant Bacterial Biofilms without Accumulated Resistance. *J. Am. Chem. Soc.* **2018**, *140* (19), 6176–6182.
- 19. Gupta, A.; Landis, R. F.; Li, C. H.; Schnurr, M.; Das, R.; Lee, Y. W.; Yazdani, M.; Liu, Y.; Kozlova, A.; Rotello, V. M. Engineered Polymer Nanoparticles with Unprecedented Antimicrobial Efficacy and Therapeutic Indices against Multidrug-Resistant Bacteria and Biofilms. *J. Am. Chem. Soc.* **2018**, *140* (38), 12137–12143.
- 20. Oz, Y.; Nabawy, A.; Fedeli, S.; Gupta, A.; Huang, R.; Sanyal, A.; Rotello, V. M. Biodegradable Poly(Lactic Acid) Stabilized Nanoemulsions for the Treatment of Multidrug-Resistant Bacterial Biofilms. *ACS Appl. Mater. Interfaces* **2021**, *13* (34), 40325–40331.
- 21. Nabawy, A.; Makabenta, J. M.; Schmidt-Malan, S.; Park, J.; Li, C. H.; Huang, R.; Fedeli, S.; Chattopadhyay, A. N.; Patel, R.; Rotello, V. M. Dual Antimicrobial-Loaded Biodegradable Nanoemulsions for Synergistic Treatment of Wound Biofilms. *J. Control. Release* **2022**, *347*, 379–388.
- 22. Kalita, S.; Kandimalla, R.; Devi, B.; Kalita, B.; Kalita, K.; Deka, M.; Chandra Kataki, A.; Sharma, A.; Kotoky, J. Dual Delivery of Chloramphenicol and Essential Oil by Poly-ε-Caprolactone-Pluronic Nanocapsules to Treat MRSA-Candida Co-Infected Chronic Burn Wounds. *RSC Adv.* **2017**, *7* (3), 1749–1758.
- 23 Worthington, R. J.; Melander, C. Combination Approaches to Combat Multidrug-Resistant Bacteria. *Trends Biotechnol.* **2013**, *31* (3), 177–184.
- 24. Shao, Z.; Wulandari, E.; Lin, R. C. Y.; Xu, J.; Liang, K.; Wong, E. H. H. Two plus One: Combination Therapy Tri-Systems Involving Two Membrane-Disrupting Antimicrobial Macromolecules and Antibiotics. *ACS Infect. Dis.* **2022**, *8* (8), 1480–1490.
- 25. Koo, H.; Allan, R. N.; Howlin, R. P.; Stoodley, P.; Hall-Stoodley, L. Targeting Microbial Biofilms: Current and Prospective Therapeutic Strategies. *Nat. Rev. Microbiol.* **2017**, *15* (12), 740–755.
- 26. Namivandi-Zangeneh, R.; Wong, E. H. H.; Boyer, C. Synthetic Antimicrobial Polymers in Combination Therapy: Tackling Antibiotic Resistance. *ACS Infect. Dis.* **2021**, *7* (2), 215–253.
- 27. Bruna, T.; Maldonado-Bravo, F.; Jara, P.; Caro, N. Silver Nanoparticles and Their Antibacterial Applications. *Int. J. Mol. Sci.* **2021**, *22* (13).
- 28. Yin, I. X.; Zhang, J.; Zhao, I. S.; Mei, M. L.; Li, Q.; Chu, C. H. The Antibacterial Mechanism of Silver Nanoparticles and Its Application in Dentistry. *Int. J. Nanomedicine* **2020**, *15*, 2555–2562.
- 29. Sangsuwan, A.; Kawasaki, H.; Matsumura, Y.; Iwasaki, Y. Antimicrobial Silver Nanoclusters Bearing Biocompatible Phosphorylcholine-Based Zwitterionic Protection. *Bioconjug. Chem.* **2016**, *27* (10), 2527–2533.
- 30. Tominaga, C.; Shitomi, K.; Miyaji, H.; Kawasaki, H. Antibacterial Photocurable Acrylic Resin Coating Using a Conjugate between Silver Nanoclusters and Alkyl Quaternary Ammonium. *ACS Appl. Nano Mater.* **2018**, *I* (9), 4809–4818.

- 31. Haidari, H.; Bright, R.; Kopecki, Z.; Zilm, P. S.; Garg, S.; Cowin, A. J.; Vasilev, K.; Goswami, N. Polycationic Silver Nanoclusters Comprising Nanoreservoirs of Ag+Ions with High Antimicrobial and Antibiofilm Activity. *ACS Appl. Mater. Interfaces* **2022**, *14* (1), 390–403.
- 32. Liao, C.; Li, Y.; Tjong, S. C. Bactericidal and Cytotoxic Properties of Silver Nanoparticles. *Int. J. Mol. Sci.* **2019**, *20* (2).
- 33. Li, C. H.; Landis, R. F.; Makabenta, J. M.; Nabawy, A.; Tronchet, T.; Archambault, D.; Liu, Y.; Huang, R.; Golan, M.; Cui, W.; Mager, J.; Gupta, A.; Schmidt-Malan, S.; Patel, R.; Rotello, V. M. Nanotherapeutics Using All-Natural Materials. Effective Treatment of Wound Biofilm Infections Using Crosslinked Nanoemulsions. *Mater. Horizons* **2021**, *8* (6), 1776–1782.
- 34. Nabawy, A.; Makabenta, J. M.; Li, C. H.; Park, J.; Chattopadhyay, A. N.; Schmidt-Malan, S.; Gupta, A.; Patel, R.; Rotello, V. M. Activity of Biodegradable Polymeric Nanosponges against Dual-Species Bacterial Biofilms. *ACS Biomater. Sci. Eng.* **2020**.
- 35. Jeyakumar, G. E.; Lawrence, R. Mechanisms of Bactericidal Action of Eugenol against Escherichia Coli. *J. Herb. Med.* **2021**, *26*, 100406.
- 36. Hemaiswarya, S.; Doble, M. Synergistic Interaction of Eugenol with Antibiotics against Gram Negative Bacteria. *Phytomedicine* **2009**, *16* (11), 997–1005.
- 37. Silva, F.; Ferreira, S.; Duarte, A.; Mendona, D. I.; Domingues, F. C. Antifungal Activity of Coriandrum Sativum Essential Oil, Its Mode of Action against Candida Species and Potential Synergism with Amphotericin B. *Phytomedicine* **2011**, *19* (1), 42–47.
- 38. Perugini Biasi-Garbin, R.; Saori Otaguiri, E.; Morey, A. T.; Fernandes Da Silva, M.; Belotto Morguette, A. E.; Armando Contreras Lancheros, C.; Kian, D.; Perugini, M. R. E.; Nakazato, G.; Durán, N.; Nakamura, C. V.; Yamauchi, L. M.; Yamada-Ogatta, S. F. Effect of Eugenol against Streptococcus Agalactiae and Synergistic Interaction with Biologically Produced Silver Nanoparticles. *Evidence-based Complement. Altern. Med.* **2015**, *2015*.
- 39. Wang, Y. ming; Kong, L. cong; Liu, J.; Ma, H. xia. Synergistic Effect of Eugenol with Colistin against Clinical Isolated Colistin-Resistant Escherichia Coli Strains. *Antimicrob. Resist. Infect. Control* **2018**, *7* (1), 1–9.
- 40. Jafri, H.; Banerjee, G.; Khan, M. S. A.; Ahmad, I.; Abulreesh, H. H.; Althubiani, A. S. Synergistic Interaction of Eugenol and Antimicrobial Drugs in Eradication of Single and Mixed Biofilms of Candida Albicans and Streptococcus Mutans. *AMB Express* **2020**, *10* (1).
- 41. Díez, I.; Jiang, H.; Ras, R. H. A. Enhanced Emission of Silver Nanoclusters through Quantitative Phase Transfer. *ChemPhysChem* **2010**, *11* (14), 3100–3104.
- 42. Kumar, A.; Joshi, H.; Pasricha, R.; Mandale, A. B.; Sastry, M. Phase Transfer of Silver Nanoparticles from Aqueous to Organic Solutions Using Fatty Amine Molecules. *J. Colloid Interface Sci.* **2003**, *264* (2), 396–401.
- 43. Noel, D. J.; Keevil, C. W.; Wilks, S. A. Synergism versus Additivity: Defining the Interactions between Common Disinfectants. *mBio* **2021**, *12* (5), e02281-21.
- 44. Matarazzo, L.; Casilag, F.; Porte, R.; Wallet, F.; Cayet, D.; Faveeuw, C.; Carnoy, C.; Sirard, J.-C. Therapeutic Synergy Between Antibiotics and Pulmonary Toll-Like Receptor 5 Stimulation in Antibiotic-Sensitive or -Resistant Pneumonia. *Front. Immunol.* **2019**, *10*

- 45. Hsieh, M. H.; Yu, C. M.; Yu, V. L.; Chow, J. W. Synergy Assessed by Checkerboard a Critical Analysis. *Diagn. Microbiol. Infect. Dis.* **1993**, *16* (4), 343–349.
- 46. Bellio, P.; Fagnani, L.; Nazzicone, L.; Celenza, G. New and Simplified Method for Drug Combination Studies by Checkerboard Assay. *MethodsX* **2021**, *8*, 101543.
- 47. Li, B.; Wang, J. H.-C. Fibroblasts and Myofibroblasts in Wound Healing: Force Generation and Measurement. *J. Tissue Viability* **2011**, *20* (4), 108–120.
- 48. Stiefel, P.; Schmidt-Emrich, S.; Maniura-Weber, K.; Ren, Q. Critical Aspects of Using Bacterial Cell Viability Assays with the Fluorophores SYTO9 and Propidium Iodide. *BMC Microbiol.* **2015**, *15* (1), 1–9
- 49. Thermo Fisher Scientific. FilmTracer TM LIVE / DEAD ® Biofilm Viability Kit. *Image (Rochester, N.Y.)* **2019**, 1–4.
- 50. Elhakim, Y. A.; Ali, A. E.; Hosny, A. E. D. M. S.; Abdeltawab, N. F. Zinc Deprivation as a Promising Approach for Combating Methicillin-Resistant Staphylococcus Aureus: A Pilot Study. *Pathogens* **2021**, *10* (10), 1–20.
- 51. Formosa-Dague, C.; Speziale, P.; Foster, T. J.; Geoghegan, J. A.; Dufrêne, Y. F. Zinc-Dependent Mechanical Properties of Staphylococcus Aureus Biofilm-Forming Surface Protein SasG. *Proc. Natl. Acad. Sci. U. S. A.* **2016**, *113* (2), 410–415.